Cell Reports, Volume *30*

Supplemental Information

Topography in the Bursting Dynamics of Entorhinal Neurons

Jason S. Bant, Kiah Hardcastle, Samuel A. Ocko, and Lisa M. Giocomo

1065

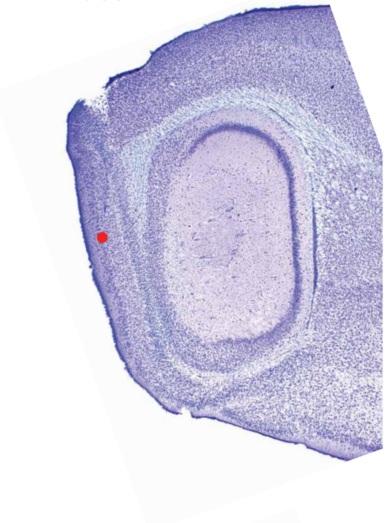

4291

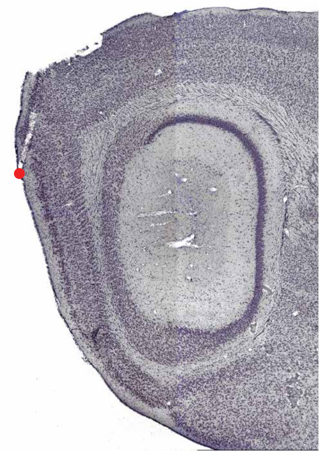

1075

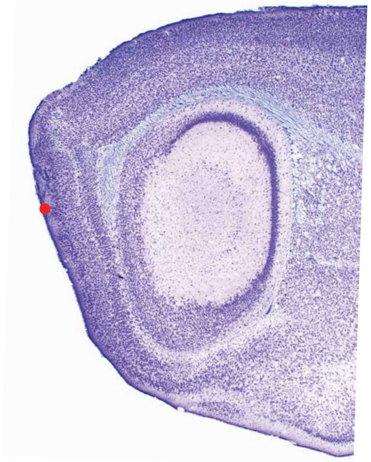

1070

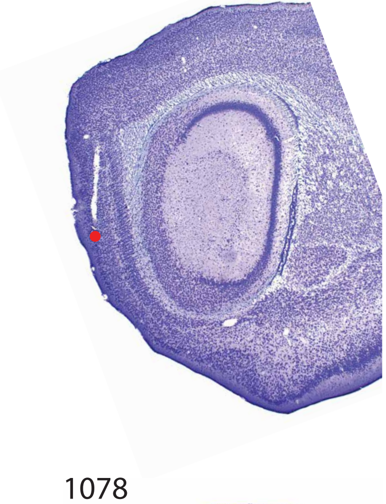

2996

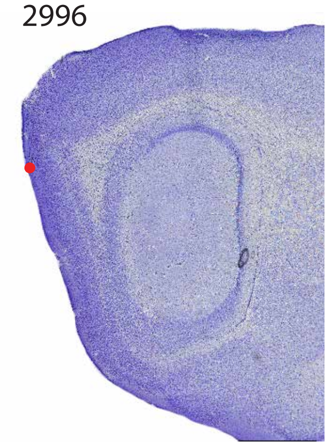

1088

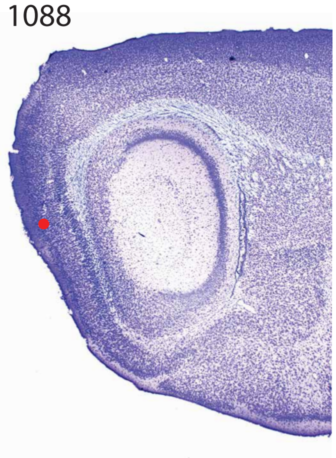

1078

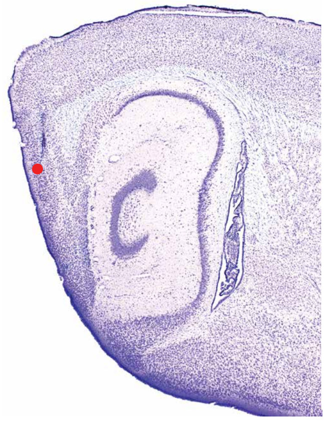

2951

2934

2938

2959

Figure S1, Related to Figures 1 and 2: Histology for 11 mice, which were representative of the recording locations for all mice included in the in vivo analysis. Nissl stained sagittal sections of the section showing the final location of the tetrode track shown. A red dot indicates the deepest ventral location of the tetrode track.

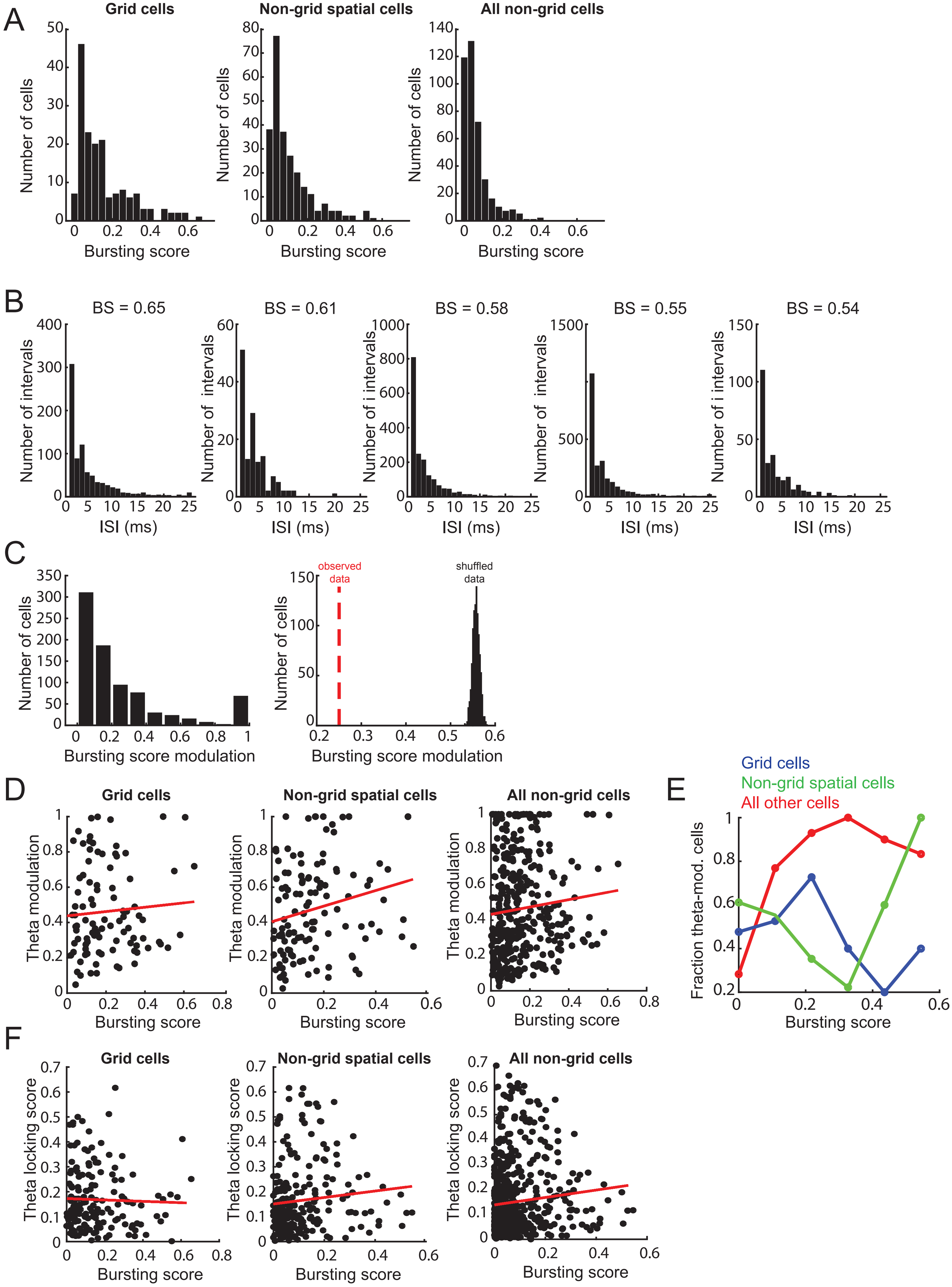
A
Grid cells
Non-grid spatial cells
All non-grid cells
Number of cells
Bursting score
0
0.2
0.4
0.6
10
20
30
40
50
60
70
80
100
120
140
B
BS = 0.65
BS = 0.61
BS = 0.58
BS = 0.55
BS = 0.54
Number of intervals
Number of intervals
Number of i intervals
Number of intervals
Number of i intervals
ISI (ms)
0
5
10
15
20
25
100
200
300
400
500
600
800
1000
1500
150
C
Number of cells
Bursting score modulation
observed data
shuffled data
0
50
100
150
200
250
300
350
0.2
0.3
0.4
0.5
0.6
0.8
1
D
Grid cells
Non-grid spatial cells
All non-grid cells
Theta modulation
Bursting score
E
Grid cells
Non-grid spatial cells
All other cells
Fraction theta-mod. cells
Bursting score
F
Grid cells
Non-grid spatial cells
All non-grid cells
Theta locking score
Bursting score
0.1
0.2
0.3
0.4
0.5
0.6
0.7

Figure S2, Related to Figures 1 and 2: Bursting dynamics in entorhinal cortex. **A.** Histogram of bursting scores observed for grid cells (left), all non-grid, non-border spatial cells (middle), and all other cells (non-grid). **B.** Histogram of the interspike intervals observed for 5 grid cells with the highest bursting scores (noted above each plot). **C.** Left: Histogram of bursting score modulation values for all cells. The bursting score modulation was computed by dividing each session into halves, computing the bursting score for each half, and then computing the absolute difference, divided by the sum, of the two bursting scores. Modulation values scale between 0 and 1, although many cells had low bursting score modulation values (mean = 0.25). Right: Comparison of the average bursting score modulation (denoted by the red dashed line) with a null distribution of average bursting score modulation values. This distribution was generated by shuffling the bursting score modulation values across the first half of all sessions, and re-computing the bursting score modulation value. The observed average lies far to the left of the null distribution, indicating that bursting scores are much more stable across sessions than would be expected if there was no stability of bursting scores. **D.** Theta modulation values versus bursting score for grid cells (left), non-grid, non-border spatial cells (middle), and all other cells (right). The theta modulation values were computed following Climer et al., 2015 (and using the code available at github.com/jrclimer/mle-rhythmicity). Following Climer et al., 2015, we compute the magnitude of rhythmicity, termed a, based on the value of these parameters: $a = (1 - b)r$, where b is a baseline likelihood and r is a rhythmicity factor. This measure varies between 0 and 1, where 1 is maximally rhythmic. We did not observe a significant correlation in grid cells (correlation coefficient = 0.071, p = 0.49) or non-grid cells (correlation coefficient = 0.097, p = 0.07), but we did see a significant relationship in non-grid spatial cells (correlation coefficient = 0.22, p = 0.015). **E.** The fraction of cells with significant rhythmicity as a function of bursting score. Following Climer et al., 2015, we compute the p-value from the log-likelihood ratio test between the rhythmic and non-rhythmic models. We then bin the bursting scores into six bins, compute the fraction of cells with $p < 0$ in each bin, and determine whether the fraction of significantly rhythmic cells changes with bursting score. We did not observe a relationship between the fraction of significantly rhythmic cells and bursting score in grid cells (p = 0.29), non-grid cells (p = 0.15), or non-grid spatial cells (p = 0.44). **F.** The bursting score versus theta locking score for grid cells (left), non-grid spatial cells (middle), or all non-grid cells (right). The theta locking score was computed based on a cell's spiking preference for a particular phase of the theta-filtered LFP. We did not see a significant relationship between theta locking and bursting score for grid cells (correlation coefficient = -0.032, p = 0.68) or non-grid spatial cells (correlation coefficient = 0.097, p = 0.07). However, all non-grid cells did exhibit a significant relationship between theta locking and bursting score (correlation coefficient = 0.1, p = 0.01).

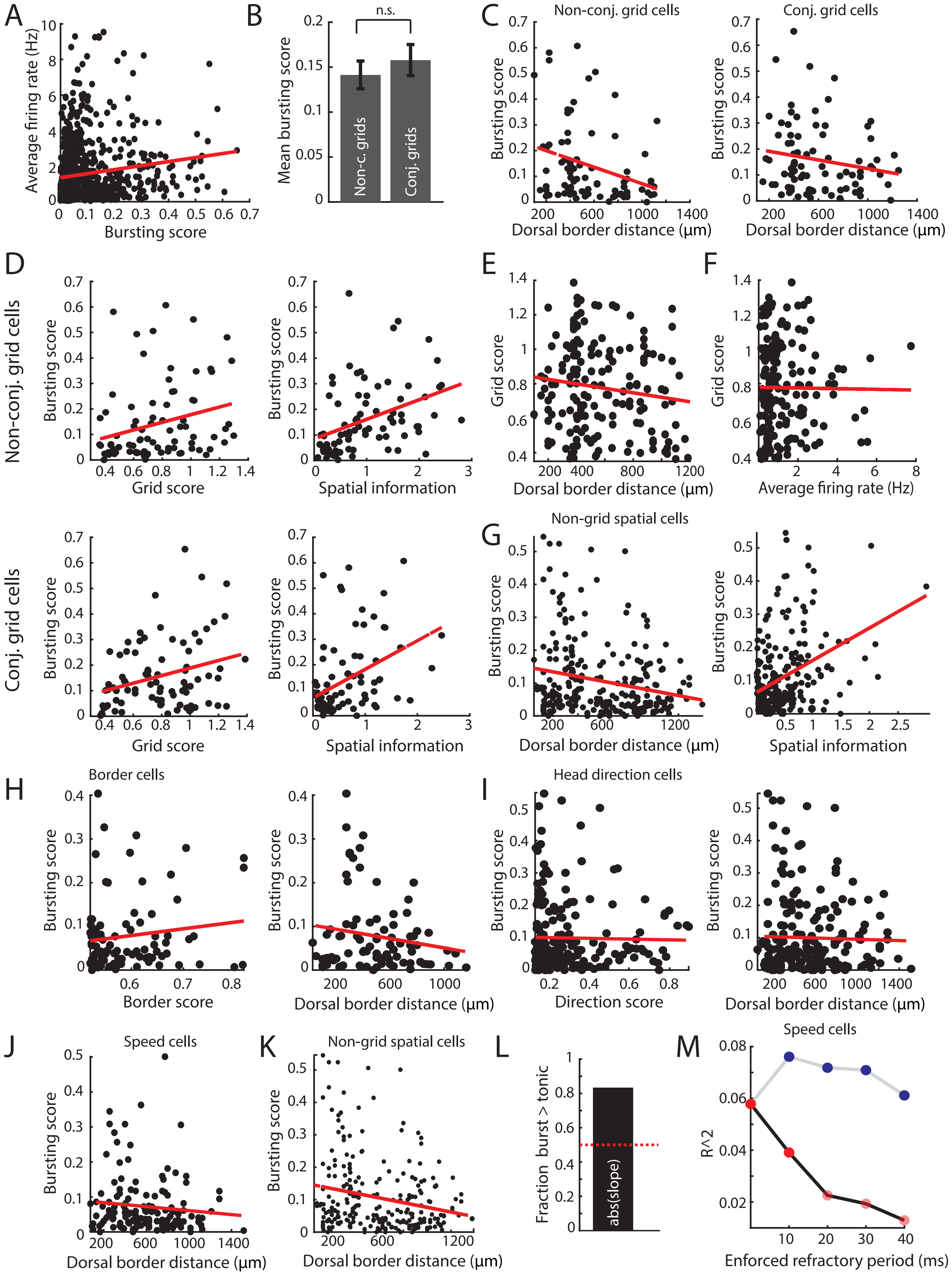
A
Average firing rate (Hz)
10
8
6
4
2
0
0 0.1 0.2 0.3 0.4 0.5 0.6 0.7
Bursting score
B
n.s.
Mean bursting score
0.2
0.15
0.1
0.05
0
Non-c. grids
Conj. grids
C
Non-conj. grid cells
Bursting score
0.7 0.6 0.5 0.4 0.3 0.2 0.1 0
200 600 1000 1400
Dorsal border distance (μm)
Conj. grid cells
Bursting score
0.7 0.6 0.5 0.4 0.3 0.2 0.1 0
200 600 1000 1400
Dorsal border distance (μm)
D
Non-conj. grid cells
Bursting score
0.7 0.6 0.5 0.4 0.3 0.2 0.1 0
0.4 0.6 0.8 1 1.2 1.4
Grid score
Bursting score
0.7 0.6 0.5 0.4 0.3 0.2 0.1 0
0 1 2 3
Spatial information
E
Grid score
1.4 1.2 1 0.8 0.6 0.4
200 400 800 1200
Dorsal border distance (μm)
F
Grid score
1.4 1.2 1 0.8 0.6 0.4
2 4 6 8
Average firing rate (Hz)
Conj. grid cells
Bursting score
0.7 0.6 0.5 0.4 0.3 0.2 0.1 0
0.4 0.6 0.8 1 1.2 1.4
Grid score
Bursting score
0.7 0.6 0.5 0.4 0.3 0.2 0.1 0
0 1 2 3
Spatial information
G
Non-grid spatial cells
Bursting score
0.5 0.4 0.3 0.2 0.1 0
200 600 1200
Dorsal border distance (μm)
Bursting score
0.5 0.4 0.3 0.2 0.1 0
0.5 1 1.5 2 2.5
Spatial information
H
Border cells
Bursting score
0.4 0.3 0.2 0.1 0
0.6 0.7 0.8
Border score
Bursting score
0.4 0.3 0.2 0.1 0
200 600 1000
Dorsal border distance (μm)
I
Head direction cells
Bursting score
0.5 0.4 0.3 0.2 0.1 0
0.2 0.4 0.6 0.8
Direction score
Bursting score
0.5 0.4 0.3 0.2 0.1 0
200 600 1000 1400
Dorsal border distance (μm)
J
Speed cells
Bursting score
0.5 0.4 0.3 0.2 0.1 0
200 600 1000 1400
Dorsal border distance (μm)
K
Non-grid spatial cells
Bursting score
0.5 0.4 0.3 0.2 0.1 0
200 600 1200
Dorsal border distance (μm)
L
Fraction burst > tonic
1 0.8 0.6 0.4 0.2 0
abs(slope)
M
Speed cells
R^2
0.08 0.06 0.04 0.02
10 20 30 40
Enforced refractory period (ms)

Figure S3, Related to Figures 1 and 2: Topographical organization in the bursting dynamics of MEC neurons. **A.** Bursting score and average firing rate are positively correlated (n = 821, R^2 = 0.021, $p < 0.001$). Red line indicates line of best fit. **B**. There was no significant difference in the bursting score between conjunctive and non-conjunctive grid cells. **C.** Non-conjunctive grid cells exhibited a strong negative correlation between bursting score and dorsal-ventral (DV) depth (left; R^2 = 0.089, $p < 0.01$), while conjunctive grid cells did not exhibit a significant negative correlation between bursting score and DV depth (right; R^2 = 0.031, p = 0.11). Red lines indicate line of best fit. However, there was no significant difference between the correlation values of the two groups (Fisher r-to-z transform: z = 0.86, p = 0.41) **D.** Top row: non-conjunctive grid cells exhibited positive correlations between bursting score and grid score (R^2 = 0.07, p = 0.02), spatial information (R^2 = 0.16, $p < 0.001$), and spatial coherence (not shown; R^2 = 0.19, $p < 0.001$). Bottom row: conjunctive grid cells exhibited positive correlations between bursting score and grid score (R^2 = 0.083, $p < 0.01$), spatial information (R^2 = 0.16, $p < 0.001$), and spatial coherence (not shown; R^2 = 0.18, $p < 0.001$). For both rows, red line indicates line of best fit. **E.** Grid score did not significantly correlate with DV depth (R^2 = 0.02, p = 0.07). Red line indicates line of best fit. **F.** While the bursting score of grid cells positively correlates with the average firing rate (R^2 = 0.08, $p < 0.001$), grid score does not correlate with the average firing rate ($R^2 = 10^{-4}$, p = 0.90). Red line indicates line of best fit. **G.** We observed a significant correlation between bursting score and the location of a non-grid spatial cell along the DV axis (R^2 = 0.05, $p < 0.01$) and between bursting score and the spatial information of a non-grid spatial cell (R^2 = 0.15, $p < 0.01$). Red line indicates line of best fit. **H.** We did not observe a correlation between the bursting score and border score of border cells (R^2 = 0.02, p = 0.22; left panel) or the bursting score and the location of a border cell along the DV axis (R^2 = 0.03, p = 0.13; right panel). Red line indicates line of best fit. **I.** We did not observe a correlation between the bursting score and mean vector length of head direction cells ($R^2 = 4*10^{-4}$, p = 0.76; left panel) or busting score and the location of a head direction cell along the DV axis ($R^2 = 8*10^{-4}$, p = 0.68; left panel). Red line indicates line of best fit. **J.** We did not observe a correlation between the bursting score and location along the DV axis for speed cells ($R^2 = 0.01$ $p = 0.23$). Red line indicates line of best fit. **K.** The dorsal-ventral position correlates with the bursting score for non-grid spatial cells ($R^2 = 0.045$, $p < 0.001$) **L.** For speed cells, bursting correlated with the absolute value of the speed cell slope (slope = firing rate x running speed; $R^2 = 0.041$, $p < 0.05$), even when the data was controlled for differences in firing rates across cells ($R^2 = 0.058$, $p < 0.01$). The absolute value of the speed slope was higher when only bursts were used, compared to when only tonic spikes were used, to compute each metric ($n = 89$, $p < 0.001$, binomial test). **M.** The squared correlation coefficient between the absolute value of the speed score, divided by average firing rate, and the bursting score of speed cells decreases as burst spikes are preferentially rejected (black line, red dots; $F(3) = 31$, $p = 0.012$). When spikes were randomly rejected, there was no significant decrease in the squared correlation coefficient between the absolute value of the speed score, divided by average firing rate, and the bursting score of speed cells (gray line, blue dots; $F(3) = 0.003$, $p = 0.96$). In addition, the slope between squared correlation coefficient and bursting score was significantly lower when burst spikes were rejected compared to when spikes were randomly rejected ($F(1) = 22$, $p = 0.004$). Transparent dots indicate non-significant correlations.

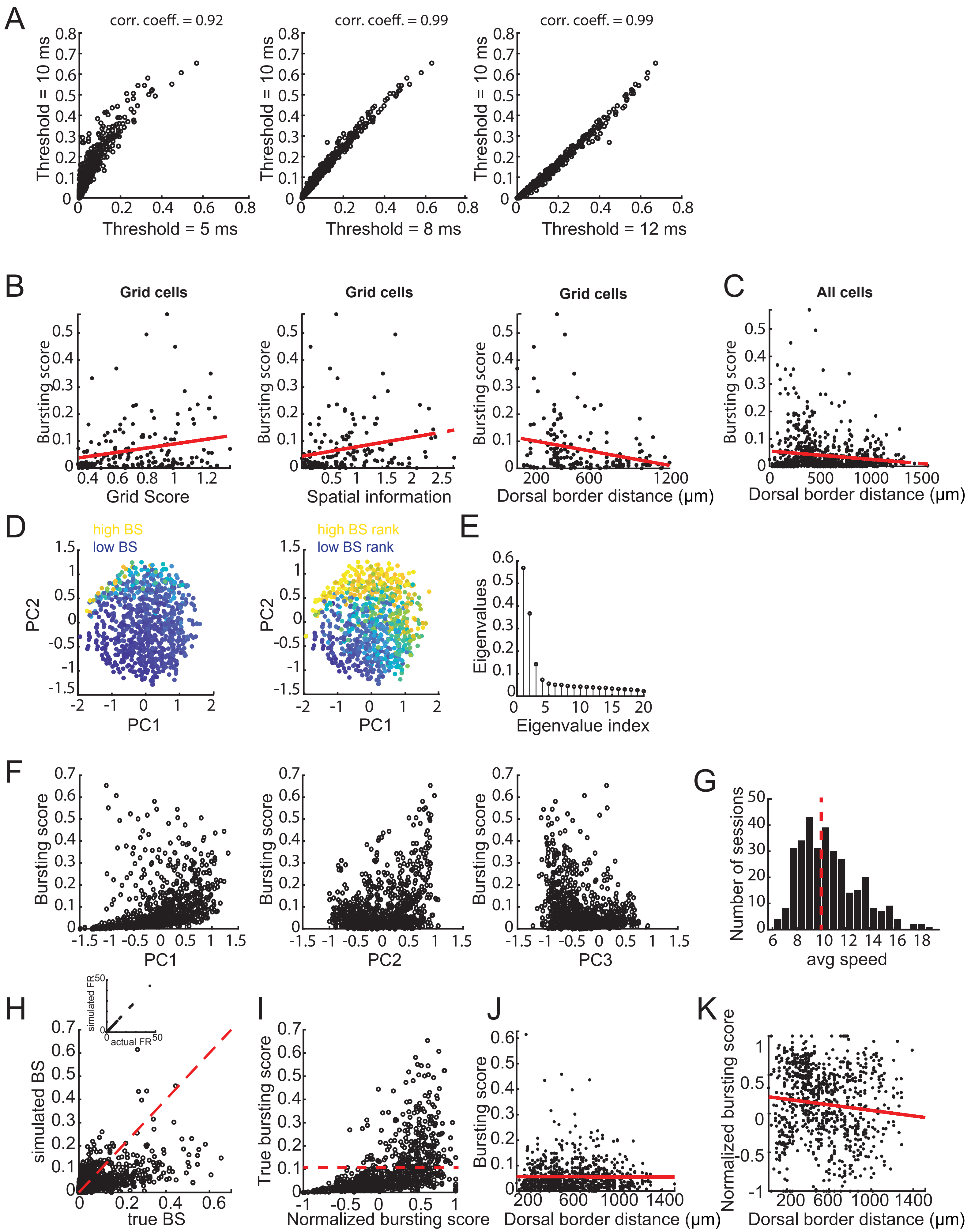

A
corr. coeff. = 0.92
corr. coeff. = 0.99
corr. coeff. = 0.99
Threshold = 10 ms
Threshold = 5 ms
Threshold = 8 ms
Threshold = 12 ms
0
0.1
0.2
0.3
0.4
0.5
0.6
0.7
0.8
B
Grid cells
Grid cells
Grid cells
C
All cells
Bursting score
Grid Score
Spatial information
Dorsal border distance (μm)
Dorsal border distance (μm)
0.4
0.6
0.8
1
1.2
0.5
1
1.5
2
2.5
200
600
1200
0
500
1000
1500
D
high BS
low BS
high BS rank
low BS rank
PC1
PC2
-2
-1
0
1
2
-1.5
-1
-0.5
0
0.5
1
1.5
E
Eigenvalues
Eigenvalue index
0
5
10
15
20
F
Bursting score
PC1
PC2
PC3
-1.5
-1
-0.5
0
0.5
1
1.5
G
Number of sessions
avg speed
6
8
10
12
14
16
18
0
10
20
30
40
50
H
simulated FR
actual FR
50
simulated BS
true BS
0
0.2
0.4
0.6
I
True bursting score
Normalized bursting score
-1
-0.5
0
0.5
1
J
Bursting score
Dorsal border distance (μm)
200
600
1000
1400
K
Normalized bursting score
Dorsal border distance (μm)
200
600
1000
1400
-1
-0.5
0
0.5
1

Figure S4, Related to Figures 1, 2 and 4: Variable bursting definitions. **A.** Comparison of the bursting score computed with a burst threshold of 10 ms with that computed with a threshold of 5 ms (left), 8 ms (middle), and 12 ms (right). In all cases, the bursting scores were highly correlated (all $p < 0.001$, correlation coefficients shown above each plot). **B.** The bursting score versus the grid score (left), spatial information (middle), and the distance from the dorsal border (right) for grid cells when the burst threshold is 5 ms. We observed significant relationships in all three plots (grid score: $p = 0.004$, spatial information: $p = 0.002$, depth: $p = 0.006$), replicating our original results with a burst threshold of 10 ms. **C.** The bursting score versus the distance from the dorsal border for all cells when the burst threshold is 5 ms. We observed a significantly negative correlation ($p = 0.00005$), replicating the results seen when the burst threshold is 10 ms. **D.** Following Latuske et al., 2015, we performed PCA on the interspike interval histograms (within a range of 0-12 ms). We then projected the data onto the first two principle components and colored each point (which corresponds to a cell) according to its bursting score (left), or its rank in a sorted list of bursting scores (right). We observed that the bursting score and the position of the neuron in the PC space were related. **E.** The eigenspectrum of the covariance matrix computed in PCA (in D). Note that the first two eigenvalues explained most of the variance. **F.** The bursting score versus the data projected on the first PC (left), the second PC (middle), or the third PC (right). The bursting score correlated with the projected data in each case (all $p < 0.001$). **G.** The distribution of average running speeds across recording sessions. The red line indicates 10 cm/s, the threshold chosen for the dividing sessions into “fast” and “slow” running speeds. **H.** The simulated bursting score versus the true bursting score. The red line indicates unity. **I.** The normalized bursting score versus the true bursting score. The red line is to aid a visual comparison of the low bursting cells (with a bursting score < 0.1) and the high bursting cells (with a high bursting score > 0.1). Note that cells with high true bursting scores (e.g. above 0.1) tended to exhibit very high normalized bursting scores, indicating that their bursting dynamics resulted from more than externally driven high firing rates. On the other hand, cells with low true bursting scores (e.g. below 0.1) tended to exhibit a range of normalized bursting scores, including negative scores that indicate that the cell bursted less than what might be expected via Poisson spiking. **J.** The dorsal-ventral distance versus the simulated bursting score. There is not a significant relationship between these two variables ($p > 0.1$). **K.** The dorsal-ventral distance versus the normalized bursting score. These are significantly related ($r^2 = 0.01$, $p = 0.001$).

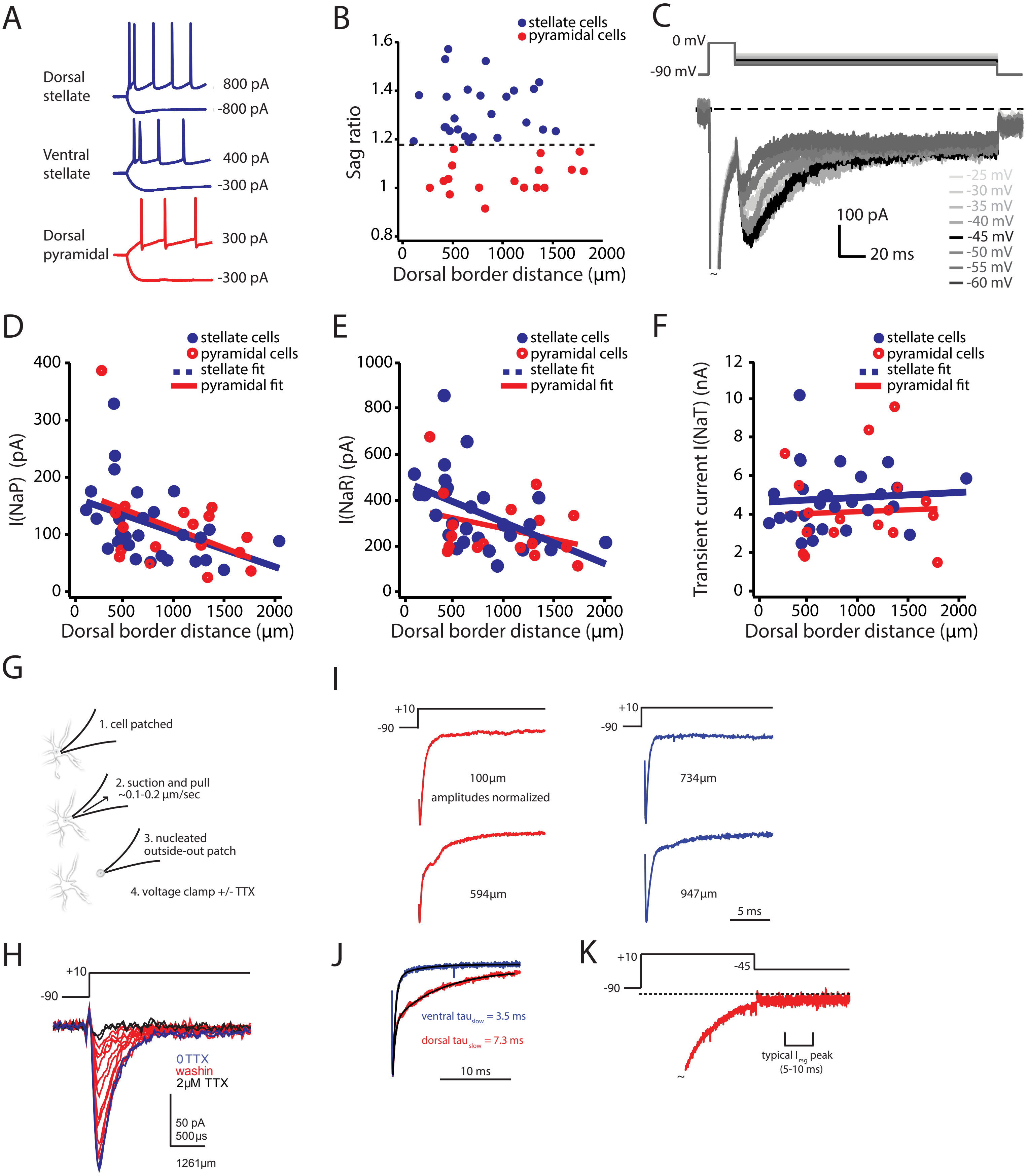
A
Dorsal stellate
800 pA
-800 pA
Ventral stellate
400 pA
-300 pA
Dorsal pyramidal
300 pA
-300 pA
B
stellate cells
pyramidal cells
Sag ratio
1.6
1.4
1.2
1
0.8
0
500
1000
1500
2000
Dorsal border distance (µm)
C
0 mV
-90 mV
100 pA
20 ms
-25 mV
-30 mV
-35 mV
-40 mV
-45 mV
-50 mV
-55 mV
-60 mV
~
D
stellate cells
pyramidal cells
stellate fit
pyramidal fit
I(NaP) (pA)
400
300
200
100
0
0
500
1000
1500
2000
Dorsal border distance (µm)
E
stellate cells
pyramidal cells
stellate fit
pyramidal fit
I(NaR) (pA)
1000
800
600
400
200
0
0
500
1000
1500
2000
Dorsal border distance (µm)
F
stellate cells
pyramidal cells
stellate fit
pyramidal fit
Transient current I(NaT) (nA)
12
10
8
6
4
2
0
0
500
1000
1500
2000
Dorsal border distance (µm)
G
1. cell patched
2. suction and pull ~0.1-0.2 µm/sec
3. nucleated outside-out patch
4. voltage clamp +/- TTX
I
+10
-90
100µm
amplitudes normalized
594µm
+10
-90
734µm
947µm
5 ms
H
+10
-90
0 TTX
washin
2µM TTX
50 pA
500µs
1261µm
J
ventral tau$_{slow}$ = 3.5 ms
dorsal tau$_{slow}$ = 7.3 ms
10 ms
K
+10
-45
-90
typical I$_{rsg}$ peak (5-10 ms)
~

Figure S5, Related to Figures 3, 4 and 5: In vitro bursting dynamics in MEC neurons. **A.** Representative current clamp recordings of the membrane potential in response to positive and negative current injections. **B.** We classified cells based on morphological and electrophysiological criteria (Alonso and Klink, 1993). To measure the sag ratio, an electrophysiological signature of MEC stellate cells, we held the membrane potential at -70 mV and applied 1 s long hyperpolarizing current steps. We classified cells as stellate when the sag ratio (sag trough/steady-state) was > 1.16 (mean sag ratio ± SEM; stellate = 1.33 ± 0.02, n = 25; pyramidal = 1.04 ± 0.02, n = 17). Sag ratios were not obtained from 3 neurons. **C.** TTX-subtracted whole-cell currents elicited with a 20-ms step to 10 mV, followed by an IV curve for repolarization to different membrane voltages. Peak I(NaR) (the black trace) is elicited at -45 mV. **D-F.** Unnormalized I(NaP) and I(NaR) amplitudes decrease along the DV MEC axis, while the transient current (I(NaT)) does not change along the same axis. This indicates that the I(NaR) and I(NaP) DV gradients reflect changes in ion channel gating kinetics rather than systematic series resistance errors or DV changes in the transient Na currents. **D.** Raw I(NaP) density in stellate (blue) and pyramidal (red) neurons plotted relative to the cell's position along the DV axis (stellate $R^2 = 0.17$, $p = 0.03$, $n = 28$; pyramidal $R^2 = 0.18$, $p = 0.09$, $n = 17$; combined $R^2 = 0.17$, $p = .005$). Best fit lines to data are shown. **E.** Raw I(NaR) density in stellate (blue) and pyramidal (red) neurons plotted relative to the cell's position along the DV axis (stellate $R^2 = 0.24$, $p = 0.008$, $n = 28$; pyramidal $R^2 = 0.10$, $p = 0.21$, $n = 17$; combined $R^2 = 0.21$, $p = 0.002$). Best fit lines to data are shown. **F.** Transient current amplitudes (I(NaT) are shown for stellate (blue) and pyramidal (red) neurons plotted relative to the cell's position along the DV axis. There was no significant correlation in I(NaT) and DV position for either stellate or pyramidal cells (stellate $R^2 = 0.005$, $p = 0.71$, $n = 28$; pyramidal $R^2 = 0.002$, $p = 0.86$, $n = 17$; combined $R^2 = 0.001$, $p = 0.83$). **G.** Somatic sodium currents in nucleated patches exhibit no I(NaR) but suggest a gradient in I(NaP) current kinetics. Previous work has suggested that some cell types express I(NaR) or I(NaP) preferentially in the axon initial segment through the first node of Ranvier (Castelli et al., 2007; Khaliq et al., 2003; Kole, 2011). Thus, it is possible that the slicing angle of our preparation results in differences in compartment-specific kinetics preservation, which could drive DV differences in the non-inactivating current densities we observe. To garner data about purely somatic currents while preserving information regarding their DV MEC position, we made outside-out macropatch recordings (Sather et al., 1992). Schematic shown here illustrates the procedure to obtain such voltage clamp recordings. **H.** Raw unfiltered recordings of currents elicited from a nucleated patch showing full “best case” subtraction quality in a ventral cell. Subtraction of the TTX recording removes leak and capacitance currents as well as other voltage dependent currents not sensitive to TTX, leaving raw voltage-gated Na currents. The initial trace is shown in blue, as TTX washes in traces are depicted in red and complete Na current block shown in black. **I.** Representative voltage-clamp recording of TTX-sensitive Na currents in nucleated patches along the DV axis. Because of the potential for small drifts in baseline on the order of the currents of interest (1-10pA), subtraction artifacts and baseline have been blanked for clarity and currents have been normalized to allow for comparison of kinetics. The late transient current decay kinetics suggested dorsal-ventral differences in persistence of opening, a signature of non-inactivating channels. **J.** Averaged normalized currents in dorsal (< 725 µm from the dorsal border, red, n = 6) or ventral (> 725 µm from the dorsal border, blue, n = 5) cells. A bi-exponential fit is shown for each set of currents to quantify persistence as measured by delayed inactivation kinetics. Both dorsal and ventral currents exhibited two components of current decay. Typical fast inactivation kinetics (first exponential of bi-exponential fit, tau = 0.4 ms) were observed in both groups but the slow component amplitudes and kinetics differed across groups. Dorsal cells exhibited ~40% of the current with a slow 7.3 ms decay tau. Ventral cells in contrast exhibited ~10% of their current with a 3.5 ms decay. **K.** Resurgent current voltage protocol was used to assay I(NaR) but no detectable current was observed upon repolarization in our patches. Averaged trace of all cells shows no peak of current 5 – 10 ms following repolarization, the window in which I(NaR) would be detected as a slowly rising transient current (bracket). Thus, in summary, we found that resurgent currents were not somatic in origin but that somatic transient Na current decay kinetics (indicative of potential delayed activation, delayed inactivation, and/or re-opening) are likely to vary in a dorsal-ventral fashion (Magistretti et al., 2003; Raman and Bean, 2001).